ACS APPLIED MATERIALS & INTERFACES

Research Article

www.acsami.org

Mussel-Inspired Electrospun Nanofibers Functionalized with Size-Controlled Silver Nanoparticles for Wound Dressing Application

Amin GhavamiNejad,*[,†,¶] Afeesh Rajan Unnithan,[†,¶] Arathyram Ramachandra Kurup Sasikala,[†] Melisa Samarikhalaj,[†] Reju George Thomas,[§] Yong Yeon Jeong,[§] Saeed Nasseri,[⊥] Priya Murugesan,[⊥] Dongmei Wu,[⊥] Chan Hee Park,*[,‡] and Cheol Sang Kim*[,†,‡]

[†]Department of Bionanosystem Engineering Graduate School and [‡]Division of Mechanical Design Engineering, Chonbuk National University, Jeonju City 561-756, Republic of Korea

[§]Department of Radiology, Chonnam National University Hwasun Hospital, Chonnam National University Medical School, Gwangju 501-746, Republic of Korea

[⊥]Department of BIN Fusion Technology, Chonbuk National University, Jeonju, South Korea

Supporting Information

ABSTRACT: Electrospun nanofibers that contain silver nanoparticles (AgNPs) have a strong antibacterial activity that is beneficial to wound healing. However, most of the literature available on the bactericidal effects of this material is based on the use of AgNPs with uncontrolled size, shape, surface properties, and degree of aggregation. In this study, we report the first versatile synthesis of novel catechol moieties presenting electrospun nanofibers functionalized with AgNPs through catechol redox chemistry. The synthetic strategy allows control of the size and amount of AgNPs on the surface of nanofibers with the minimum degree of aggregation. We also evaluated the rate of release of the AgNPs, the biocompatibility of the nanofibers, the antibacterial activity in vitro, and the wound healing capacity in vivo. Our results suggest that these silver-releasing nanofibers have great potential for use in wound healing applications.

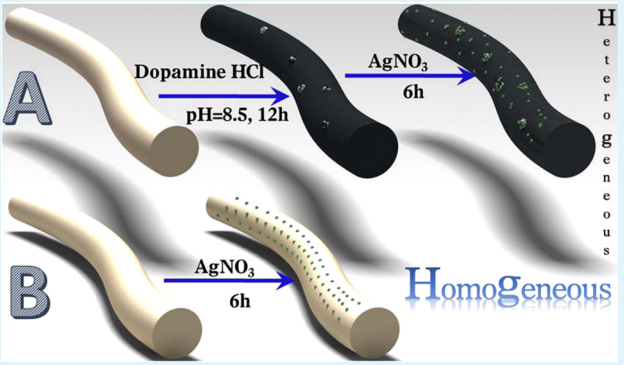

KEYWORDS: *mussel-inspired, dopamine, electrospinning, nanofiber, wound healing, silver nanoparticles*

INTRODUCTION

The skin is the largest organ in the body of vertebrates, and it is an important natural barrier to protect internal organs from chemical or mechanical damage.[1,2] To date, substantial efforts have been made to provide effective treatment for burns, abrasions, exposure to chemical/biological agents, and other skin lesions.[3,4] An ideal wound dressing should possess special properties such as good biocompatibility, sufficient physical protection of the wound site against bacterial intrusions, high porosity to allow for gas exchange, and promotion of epithelization.[5,6] To provide these properties, researchers have developed various wound dressing materials.[7,8] Among these, special attention has been paid to nanofibrous membranes that are produced by electrospinning due to their close structural resemblance to native extracellular matrix, good porosity, and high surface area-to-volume ratio that can promote hemostasis and absorb wound exudates.[7,9−13]

To prevent bacterial colonization and subsequent wound infection, antibacterial agents should also be incorporated into the polymeric nanofibers.[13,14] Of the various antimicrobial agents that are available, silver-nanoparticles (AgNPs) have been recognized to have a broad spectrum and to be highly effective antimicrobial agents when treating infectious wounds.[15] Furthermore, recent investigations have suggested that the release of AgNPs is crucial for the material to act as an antibacterial agent.[16,17] Once AgNPs are released into the surroundings of the material, they destroy the metabolic processes of bacterial cells.[18] In summary, the incorporation of releasable AgNPs into polymeric nanofibers could be a promising technique to provide effective antibacterial action during wound management.

Several techniques have been employed to incorporate AgNPs into a variety of nanofibrous scaffolds targeting antimicrobial applications.[19] Composite fibers have been synthesized by electrospinning a dispersion of previously prepared NPs in a polymer solution.[20,21] However, this approach has a limitation in that the dispersion of inorganic NPs during electrospinning results in aggregation and a quick loss of their antibacterial activity.[22,23] Therefore, the assembly of AgNPs onto nanofibers could be a good strategy to avoid

Received: March 23, 2015
Accepted: May 19, 2015
Published: May 19, 2015

DOI: 10.1021/acsami.5b02542
ACS Appl. Mater. Interfaces 2015, 7, 12176−12183

aggregation and to enhance their antibacterial activity.[24−26] Messersmith et al. investigated mussel adhesion in nature and found that under alkaline conditions, dopamine can self-polymerize into polydopamine (pdopa), which offers a simple method to coat various organic and inorganic substrates.[27,28] Another interesting feature of surface modification with pdopa is its unique reductive properties.[29] The pdopa coatings that formed contain catechol groups that permit the formation of metallic NPs.[30] The catechol group has a moderate capability for reduction, which is strong enough to induce the chemical reduction of metal ions including silver and gold ions.[30] Interestingly, AgNPs formed via catechol redox chemistry are not sensitive to oxygen, which allows for long-term antimicrobial activity.[31]

Despite the many advantages of the surface modification by the self-polymerization of dopamine, several barriers still prevent the full use of this technique, including the inability to control the thickness and surface morphology.[32] The self-polymerization of dopamine under alkaline conditions results in the formation of numerous unavoidable nano/microparticulate aggregates of pdopa on the surface of the materials.[33] These aggregates not only give rise to a significant increase in the surface roughness,[34] but also could cause a nonuniform dispersion of NPs after immobilization since the aggregation state of the immobilized NPs is dependent on the surface roughness.[35]

In this study, we present a facile one-step electrospinning process to synthesize electrospun mussel-inspired copolymer, poly(dopamine methacrylamide-*co*-methyl methacrylate) (MADO), with improved antibacterial activity resulting from surface functionalization with AgNPs. The assembly of the silver nanostructures is driven by the catecholic moiety of dopamine methacrylamide in polymeric backbone. The AgNPs were uniformly attached on the surface of the electrospun catecholic nanofibers in contrast with AgNPs that are assembled on pdopa-coated nanofibrous membranes through the classical approach. We evaluated the biocompatibility of the nanofibers as well as their in vitro antibacterial activity and in vivo wound healing capacity by performing a histological analysis. To the best of our knowledge, this is the first report on both the in vitro and in vivo behavior of mussel-inspired silver releasing antimicrobial polymeric fibers as a wound dressing material.

MATERIALS AND METHODS

Materials. Methacryloyl chloride, sodium borate, sodium bicarbonate, 3,4-dihydroxyphenethylamine hydrochloride, tetrahydrofuran (THF), dimethylformamide (DMF), and methyl methacrylate (MMA) were purchased from Daejung Co. Diethyl ether, methylene chloride, 2-cyano-2-propyl dodecyl trithiocarbonate (CPDB), poly methyl methacrylate (PMMA), azobis(isobutyronitrile) (AIBN), 3,4-dihydroxyphenethylamine hydrochloride, ethanol, and hexane were purchased from Sigma-Aldrich, South Korea. All aqueous solutions were prepared with ultrapure water purified with a Milli-Q UV-Plus water purification system (Millipore, Bedford, MA). The water had a resistivity of $>10^{18}$ MU cm^{-1}.

Synthesis of Dopamine Methacrylamide (DMA). The dopamine methacrylamide (DMA) monomer was prepared and characterized in accordance with a strategy that was previously reported.[36] A gray powder was produced with a yield of 80%. The structure of the monomer was confirmed via nuclear magnetic resonance spectroscopy. ^{1}H NMR (400 MHz, DMSO, 273 K), 6.4−6.6(3H, m, Ph), 5.5 (1H, d, CH_2═C−), 5.25 (1H, d, CH_2═C−), 3.3 (2H, q, CH_2−NH−), 2.5 (2H, tr, CH_2−Ph), 1.8 (3H, s, CH_3−C−).

Synthesis and Characterization of p(MMA-*co*-DMA). Synthesis of poly(methyl methacrylate-*co*-dopamine methacrylamide), abbreviated as MADO, proceeded as follows.[37] A 50 mL round-bottomed flask was used to dissolve the appropriate amount of the two monomers, MMA (47 mmol) and DMA monomer (9.4 mmol), in dry DMF. Then, the calculated volumes of stock solutions of CPDB and AIBN in DMF were added. The ratios of [M] to [CPDB] and [CPDB] to [AIBN] were 150:1 and 4:1, respectively. The mixture was deoxygenated with nitrogen bubbling for 30 min. The reaction was performed in an oil bath at 70 °C for 17 h. The samples were periodically withdrawn to measure the monomer conversion via ^{1}H NMR. The reaction mixture was added dropwise to 400 mL of diethyl ether under stirring to precipitate the synthesized copolymer, and the obtained copolymer was dissolved in methylene chloride and was precipitated in diethyl ether twice to obtain a pure copolymer. The purified copolymer was dried under vacuum until a constant weight was achieved (70% yield). The copolymer had a relatively large molecular weight of approximately 16 000 g/mol and a fairly narrow molar mass distribution of 1.2. ^{1}H NMR (250 MHz, DMSO): δ 8.70(s, 1H, −OH), 8.60 (s, 1H, −OH), 6.6−6.4 (m, 3H, Ar−H), 3.50 (s15H,-O−CH_3), 3.24 (m, 2H, Ar−CH_2− CH_2(NH)−), 2.45 (m, 2H, Ar−CH_2−CH_2(NH)−), 1.2−0.9 (m,18H, -C−CH_3).

Fabrication of Catecholic Nanofibers MADO. The copolymer solutions were prepared by dispersing the polymer at a concentration of 25 wt % in DMF. The resulting solutions were placed in a plastic syringe tube and fed through a metal capillary (nozzle) with a diameter *di* = 0.21 mm (21 G) attached to a 1-D robot-system that moves laterally. The system was controlled with the LabVIEW 9.0 software (National Instruments). The feeding rate was maintained at 0.5 mL/h through the use of a controllable syringe pump. Electrospinning was carried out at room temperature with a voltage of 18 kV and a working distance of 15 cm. The nanofibers were then vacuum-dried for 24 h to remove the residual solvent, and these samples were then used for further studies. The single absorbance peak appeared in ultraviolet−visible (UV−vis) spectroscopy at 280 nm, and the absence of additional peaks at wavelengths longer than 300 nm showed that the catechol groups were not oxidized during the electerospining process (Figure S1, Supporting Information).

On-Surface Synthesis of AgNPs on MADO Nanofibers (MADO-AgNPs). In a typical procedure, the electrospun catecholic nanofibers (MADO, 5 cm × 5 cm) were weighted and carefully dipped into 20 mL of 1 mM $AgNO_3$ in deionized water. The samples were mildly shaken at room temperature for 6−24 h. AgNPs progressively formed, and the color of the fiber mats evolved from white into dark yellow. The samples were then rinsed with an excess amount of deionized water and were subsequently dried in a vacuum.

Preparation of AgNPs on Polydopamine-Coated Nanofibers (Ag-Pdopa Coated Sample). The pdopa-coated nanofibrous membranes were prepared simply by following the universal method where pure PMMA nanofibers are immersed in aqueous Tris−HCl buffer solution and are then mixed with dopamine (2 mg of dopamine per milliliter of 10 mM Tris−HCl, pH = 8.5) for about 12 h. Rinsing with an excess amount of deionized water then followed. In the next step, the pdopa-coated nanofibers were immersed into a 1 mM mixture solution of silver ions with mild shaking in a shaking incubator at 37 °C for 6−24 h. AgNPs progressively formed, and the color of the fiber mats evolved from brown into black. The samples were then rinsed with an excess amount of deionized water and were subsequently dried in a vacuum.

Characterization. The surface structure and morphology of the as-prepared MADO and MADO-AgNPs nanofibers were studied via field-emission scanning electron microscopy (FESEM; Zeiss Supra 40VP) and transmission electron microscopy (TEM, JEOL JEM, Japan), respectively. X-ray powder diffraction (XRD) analyses of the AgNPs and MADO-AgNPs were carried out by using a Rigaku X-ray diffractometer (Cu Kα, λ = 1.54059 Å) over Bragg angles ranging from 10−90° to study the crystalline structure of the materials. In addition, the exact sizes of the resulting NPs were calculated by using the Scherrer formula in the High Score Plus software. The molecular weight (Mw) and the molecular weight distribution (M_w/M_n) of the

DOI: 10.1021/acsami.5b02542
ACS Appl. Mater. Interfaces 2015, 7, 12176−12183

copolymer samples were determined by using a size-exclusion chromatography (SEC) system equipped with a refractive index detector (PL-GPC110, Polymer laboratories). The measurements were performed in chloroform at 40 °C. Linear polystyrene standards were applied for calibration, and the bonding configurations of the samples were characterized by means of their Fourier transform infrared (FTIR) spectra using a Paragon 1000 Spectrometer (PerkinElmer). The elemental composition and surface state of the samples were checked using X-ray photoelectron spectroscopy (XPS, AXIS-NOVA, Kratos, Inc.) with an Al Kα irradiation source. The amount of silver released from the electrospun membranes was analyzed via inductively coupled plasma mass spectrometry (ICP-MS). The samples were cut into 5 × 5 cm^2 pieces. After the weight measurements, the specimens were placed into a centrifugation tube with 10 mL of phosphate-buffered saline (PBS) and were then incubated for 1 week at 37 °C. Two and one-half milliliters of the released solution were extracted at different time intervals and were digested overnight with nitric acid at a 1:1 ratio by volume. Calibration was conducted using an external standard between 1 and 200 ppb. The viability of the cultured NIH3T3-L1 fibroblasts (preadipocytes, Korean Cell Line Bank, Korea) was monitored on the first and third day of culture using the colorimetric MTT assay (Sigma, USA). The nanofiber scaffolds were washed twice with PBS and were then treated with approximately 50 μL of MTT solution (DMEM). The contents were mixed by side-tapping, and the scaffolds were then incubated at 37 °C for 2 h. The nanofiber scaffolds containing the MTT-cell mixtures were gently rocked to deposit the cells. The supernatant of the MTT solution was pipetted out, and then acid–isopropanol (95 mL isopropanol with 5 mL 3 N HCl) was added to the colored cell deposit. After scaffolds treated with acid-alcohol were mixed gently, the samples were then allowed to react for 5 min. One-hundred microliters of purple–blue colored supernatant containing the solubilized formazan from each sample was added to a well of a 96-well plate for an enzyme-linked immunosorbent assay (ELISA) analysis at 580 nm. The cell viability was obtained by comparing the absorbance of the cells cultured on the nanofiber scaffolds to that of control wells containing cells. The results were expressed as the mean ± standard error of the mean. The data were analyzed using Student's t test and repeated measures of analysis of variance (ANOVA) test. A probability of less than 0.01 was considered to be statistically significant. The in vivo animal study was approved by the Institutional Animal Ethical Committee, IACUC at Chonbuk National University, Jeonju, South Korea (certification number CBU 2014–00062). Wistar rats weighing from 200–250 g and between 4 and 6 weeks of age were used in this study. All of the animals were fed with commercial rodent chow diet and tap water ad libitum. The rats were housed in a room at a constant temperature (22 ± 1 °C) and humidity (60 ± 3%) with a 12-h light/12-h dark cycle. On the day of the wound creation, the rats were anaesthetized with 80 mg/kg ketamine and 8 mg/kg xylazine in an intraperitoneal injection. The dorsal area of the rats was depilated, and the operative area of the skin was cleaned with alcohol. A partial thickness skin wound was created in a 1.5 × 1.5 cm^2 region by excising the dorsum of the rat using surgical scissors and forceps. The wounds were then covered with the MADO-AgNPs and MADO nanofibers, and the rats with bare wounds were covered with cotton gauze. After the dressing materials had been applied, the rats were housed individually in cages under normal room temperature. The dressing materials were changed at days 5, 10, and 15. When the dressings were changed, the animals' hairs were cropped to take photographs. After day 15, the skin wound tissue of the rats was excised, fixed with 10% formalin, and stained with hematoxylin–eosin (H&E) to perform histological observations.

RESULTS AND DISCUSSION

The morphologies of the MADO and MADO-AgNPs nanofibers were evaluated using FESEM. The MADO nanofibers were observed to be smooth without beads and with an average diameter of around 800 nm (Figure 1a). After incubation with the silver nitrate solution, plenty of NPs were deposited on the surface of the MADO nanofibers, indicating the successful reduction of $AgNO_3$ to metallic AgNPs (Figure 1b). Furthermore, the high-resolution transmission electron micrographs illustrate that the diameter of the AgNPs increased as the incubation time increased with a selective and uniform distribution on the surface of the polymeric nanofibers due to the presence of the catechol groups of the DMA monomer on the surface of the MADO nanofibers (Figure 1c,d,e). In contrast with the MADO nanofibers, the HR-TEM image of the Ag-pdopa coated samples (Figure 1f) clearly shows aggregated pdopa and silver particles. These aggregations might be a result of the uncontrollable surface characteristics of the oxidative self-polymerization of dopamine coating on the nanofibers. However, the HR-TEM results strongly suggest that the use of the catecholic monomer in the MADO nanofibers resulted in the synthesis of monodispersed AgNPs, while AgNPs become aggregated in the presence of melanin-like structures of the oxidized catechols in pdopa.[38]

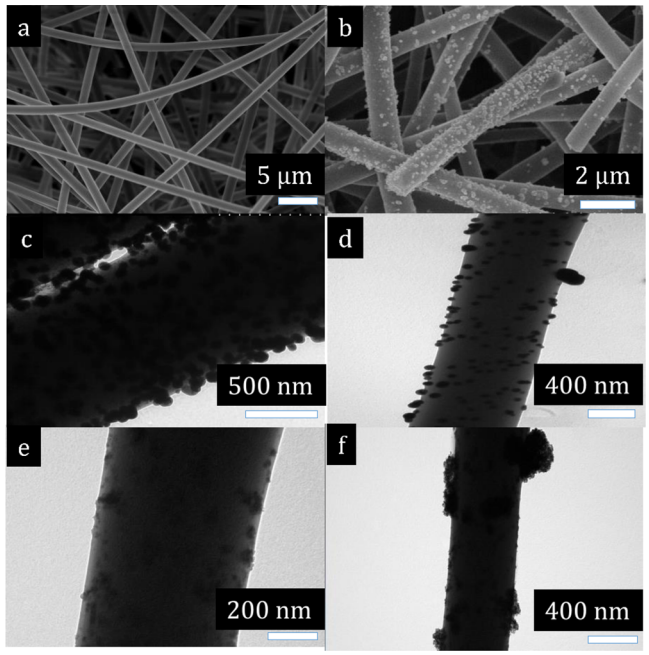

Figure 1. FESEM images of electrospun (a) MADO nanofibers and (b) MADO-AgNPs nanofibers, and HR-TEM images of MADO-AgNPs nanofibers after incubation for (c) 24 h, (d) 12 h, and (e) 6 h. HR-TEM image of Ag-pdopa-coated sample after incubation for (f) 6 h.

The XRD pattern of the AgNPs-MADO composite was analyzed to confirm the formation of AgNPs on the surface of the nanofibers (Figure 2). The peaks at 38.1°, 44.2°, 64.5°, and 77.5° correspond to the (111), (200), (220), and (311) diffractions of metallic Ag (JCPDS No. 04–0783). Furthermore, the reflections appear to be sharper for the NPs as the incubation time increases, indicating that the incubation time plays an important role in determining the size of the NPs. Assuming that the broadening of the powder diffraction peaks is only due to the crystallite size and the instrumental broadening of the diffractometer, the exact size of the obtained Ag NPs can also be calculated from the half widths of the major diffraction peaks (111) according to the Scherrer formula:

$$t = \frac{0.9\lambda}{W_{size}\cos\theta} W_{size} = W_b - W_s$$

DOI: 10.1021/acsami.5b02542
ACS Appl. Mater. Interfaces 2015, 7, 12176–12183

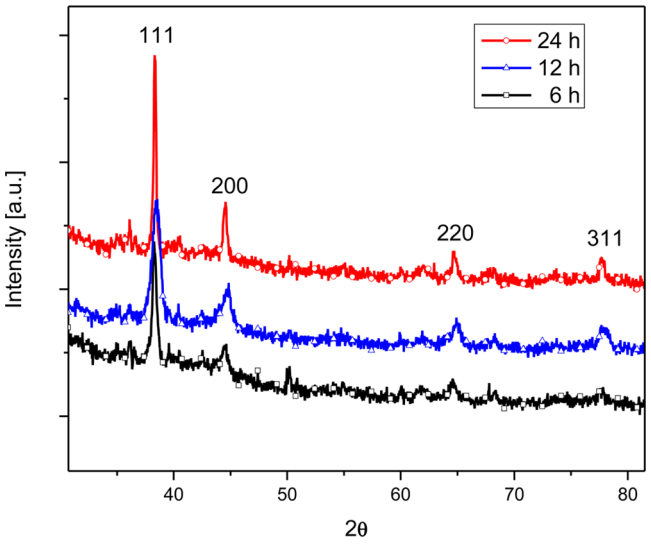

Figure 2. XRD patterns of the MADO-AgNPs nanofibers prepared using various incubation times: (a) 6h, (b) 12 h, and (c) 24 h.

Where t is the apparent size of the crystallites, λ is the wavelength of the X-ray radiation, W_{size} is the broadening caused by small crystallites, W_b is broadening profile fwhm, W_S is standard profile fwhm, and θ is the angle at which that peak is centered. The results indicate that the size of the AgNPs attached to the surface of nanofibers increased as the incubation time increased with 18 nm at 6 h, 40 nm at 12 h, and 69 nm at 24 h for MADO-AgNPs and 23 nm at 6 h, 54 nm at 12 h, and 90 nm at 24 h for the Ag-pdopa coated samples. The above results are in good agreement with the results given via FESEM and HR-TEM images.

The functionalization of the MADO nanofibers with AgNPs can also be confirmed via FTIR spectroscopy (Figure 3). In the

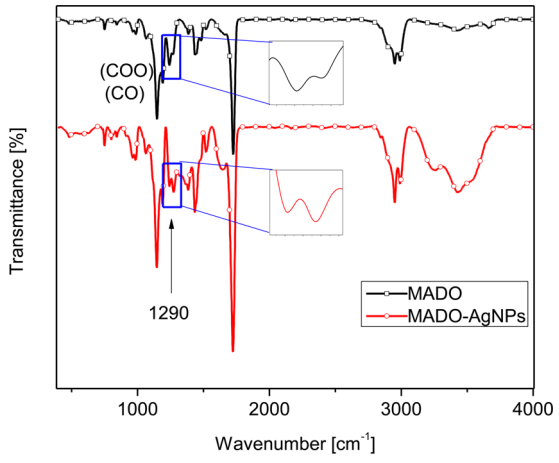

Figure 3. FTIR spectra of (a) MADO and (b) MADO-AgNPs composite nanofibers.

MADO fibers, the peak at 3440 cm^{-1} is attributed to the hydroxyl stretching vibration, the peaks at 3002 cm^{-1}, 2952 cm^{-1}, and 2842 cm^{-1} to the C−H stretching vibration, and the absorption bands at 1743 and 1436 cm^{-1} are characteristic of the −C═O and −CH2− groups of the polymer, respectively. The FTIR-spectrum bands between 1240 and 1145 cm^{-1} are mainly due to the presence of methyl ester groups, and the peaks at 984 and 840 cm^{-1} correspond to the C−H bending wagging vibration and the deformation vibration of the O−C−O bonds of the polymer. The FTIR spectrum of the MADO-AgNPs nanofibers is nearly identical to that of pure MADO fibers. However, in comparison with the FTIR spectrum of the MADO nanofibers, the intense absorption peaks at around 1620 and 3400 cm^{-1} could be ascribed to the existence of AgNPs in the composite nanofibers.[39] In addition, the IR spectrum of the composite nanofibers shows that the phenolic C−O−H stretching vibration (1290 cm^{-1}) of the catechol groups in MADO nanofibers significantly decreases when the nanofibers are treated with silver ion precursors, indicating that the oxidation of the catechol moiety in the MADO nanofibers is responsible for the reduction of the silver ions into solid AgNPs.

The chemical compositions of the MADO nanofiber and MADO-AgNPs composite nanofiber surfaces were characterized via XPS spectroscopy. The XPS wide scan data for electrospun MADO nanofibers only shows peaks for C 1s (284.7 eV), O 1s (531 eV), and N 1s (399 eV). In contrast, the XPS spectrum of MADO-AgNPs exhibits the presence of C 1s, N 1s, O 1s, Ag 3d, and Ag 3p (Ag $3p_{5/2}$, Ag $3p_{3/2}$), where the strong Ag signal peaks at a binding energy of about 370.0 eV indicate the presence of the silver element.[40] As shown in the spectrum (Figure 4, inset), two bands at about 368 and 374 eV

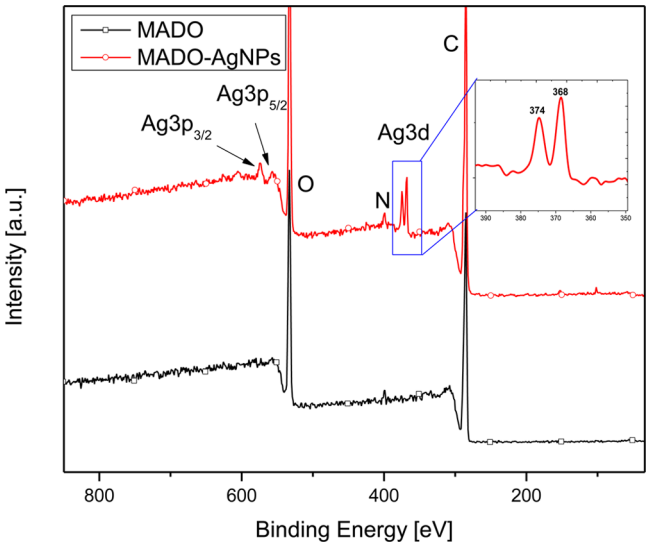

Figure 4. XPS scans of (a) MADO and (b) MADO-AgNPs composite nanofibers. (Inset: Ag 3d core−level spectrum of the MADO-AgNPs composite nanofiber).

were observed, and these are ascribed to the Ag $3d_{5/2}$ and Ag $3d_{3/2}$ binding energies, respectively.[41] The split at the 3d doublet of Ag is of 6.0 eV implies that the synthesized AgNPs were zerovalent.[42] Ag 3d5 spectroscopy was conducted through XPS experiments to determine the weight percentage of the AgNPs in the nanofibers. The content of the AgNPs in the MADO-AgNPs samples (incubation time = 6 h) was estimated to be 1%, as determined from at least 10 samples. However, the XPS results in the Ag-pdopa coated samples (prepared under the same conditions) show different weights between 1 and 4%, and there seems to be no general trend that can be used to predict the exact content of AgNPs on the surface of these samples. Such behavior could be attributed to the different arrangements of catechol moieties in the structure of pdopa, which has not yet been fully explored.

DOI: 10.1021/acsami.5b02542
ACS Appl. Mater. Interfaces 2015, 7, 12176−12183

For the pdopa-coated samples, an oxidizing agent was used, and the self-polymerization of dopamine generated many PDA macro/nano particles that aggregated on the surface of the nanofibers. Thus, the catechol groups have different efficiencies with respect to the reduction of metal ions. In the dip-coating method, some catechol groups could be covered by these particles or even by other residual monomers, which influences the controllability of the amount of NPs in this sample. In contrast, MADO-AgNPs exhibited no aggregation in their unoxidized catechol groups. Therefore, the MADO nanofibers have higher activity in terms of reduction, with great reproducibility in terms of the size and amount of AgNPs that are incorporated. These results indicate that the conditions to control the loading of AgNPs in the MADO nanofibers were significantly better than those in the Ag-pdopa coated samples; therefore, in the remainder of this work, we will focus on the MADO-AgNPs samples.

Figure 5 shows the release profile for silver from the MADO-AgNPs membrane as a function immersion time. Within the

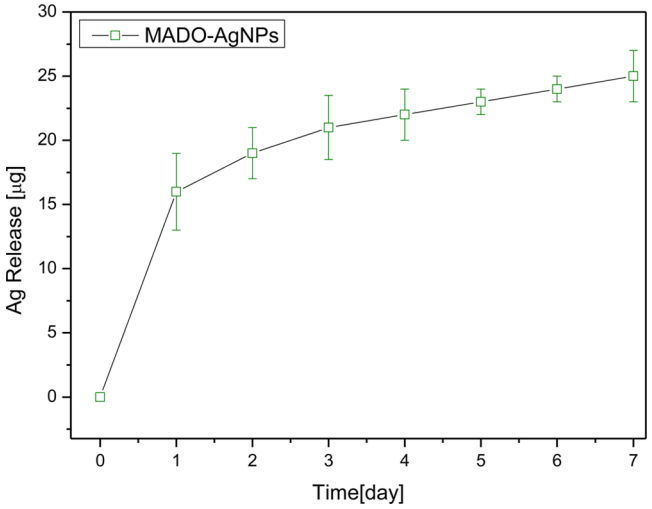

Figure 5. In vitro release profile of Ag from MADO-AgNPs scaffold as a function of time.

first day, Ag was quickly released from the sample, and then a slow sustained release was observed over the following 5 days. The initial amount of silver released from the membranes was of about 16 μg (13%), which is not known to be toxic to mammalian cells but can inhibit bacterial growth. It is also remarkable to point out that about 87% of the silver still remained in the composite 1 day after incubation, indicating that most of the AgNPs were coordinated stably with the catechol groups of the MADO nanofibers.

Nevertheless, further study is required to identify the critical factors that influence release of the AgNPs in the MADO fibers, but this rapid, constant release of Ag from the composite fiber mat could be helpful in reducing inflammation and preventing reinfection at the wound site.

The antimicrobial activity of the MADO-AgNPs nanofibers was evaluated by conducting a disc diffusion test for both Gram-negative bacteria (*Escherichia coli*) and Gram-positive bacteria (*Staphylococcus aureus* and *Pseudomonas aeruginosa*). Nanofibers without silver coatings were used as control samples, and as expected, the bactericidal activity indicated a clear zone of inhibition only around the MADO-AgNPs nanofibers, indicating that the antibacterial activity was due to the presence of AgNPs attached on the surfaces of the nanofibers (Figure 6, inset). The percentage increase of the

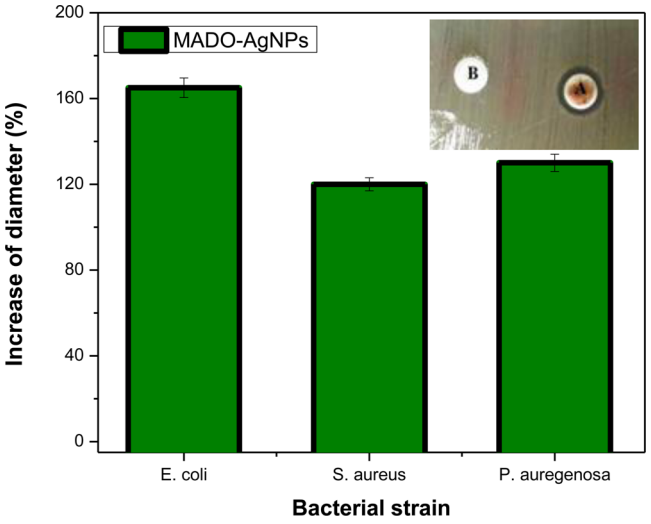

Figure 6. Results of the antibacterial activity of MADO-AgNPs electrospun membranes against *Pseudomonas aeruginosa*, *Staphylococcus aureus*, and *Escherichia coli*. The inset shows a comparison of (A) MADO-AgNPs nanofiber and (B)MADO nanofiber on a LB-agar plate covered with *Pseudomonas aeruginosa*.

diameters for each of the samples is shown in the schematic diagram in Figure 6. The values for the MADO-AgNPs nanofibers were 164, 121, and 133% for *E. coli*, *S. aureus*, and *P. auregenosa*, respectively, which indicate that the MADO-AgNPs showed better activity toward Gram-negative bacteria than Gram-positive bacteria, possibly due to the Gram-positive bacteria being protected by a thick peptidoglycan wall that limits the penetration of the AgNPs.[43] The antimicrobial activity of the MADO-AgNPs can be explained to be a result of the small AgNPs that were homogeneously distributed on the surface of the nanofibers with a minimum degree of aggregation. Furthermore, the AgNPs that are released from these samples can freely diffuse into the test media and can interact with the sulfur-containing intracellular proteins in bacteria, killing them. Therefore, the MADO-AgNPs nanofibers exhibited significant antimicrobial activity and suggest an improvement in the wound healing efficiency.

In addition to their good antibacterial activity, the biocompatibility of the nanofibers is another crucial factor that is relevant to the application of the materials as wound dressings. To this end, an MTT assay was carried out to assess the cytotoxicity of the nanofibers, and the results of this test are provided in Figure 7. As can be seen, improvements in cell proliferation and biocompatibility were observed for MADO nanofibers due to the biocompatibility and low cytotoxicity of dopamine.[44,45] The MADO-AgNPs did not exhibit significant cytotoxicity against mammalian cells, and more than 85% of the cells were still viable after incubation for 72 h. This result is consistent with a previous study by Wang et al.[46] who showed that AgNPs at a concentration of 1% did not have a significant lethal effect on cell growth.

After the antibacterial test and the evaluation of the biocompatibility, the real wound healing efficiency of the nanofibers was demonstrated by creating full thickness skin wounds on the back of rats in an in vivo experiment. Figure 8 shows optical images of the wound appearances at 5, 10, and 15

DOI: 10.1021/acsami.5b02542
ACS Appl. Mater. Interfaces 2015, 7, 12176−12183

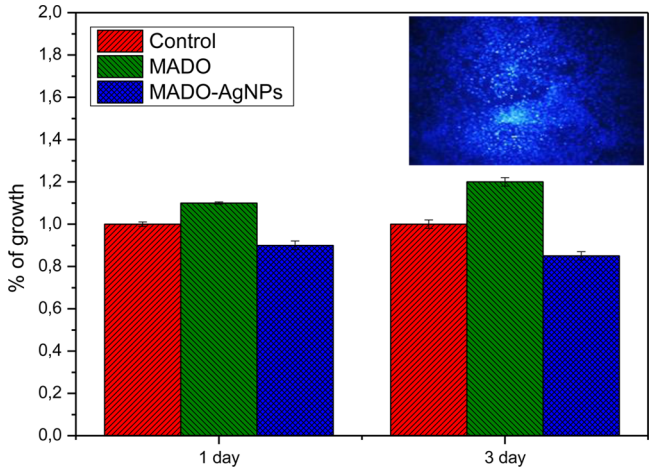

Figure 7. MTT cell growth measurement assay on NIH3T3 cell lines for MADO and MADO-AgNPs. The viability of the control cells was set at 100%, and the viability relative to control was expressed. The inset shows the cell proliferation at day 3 for the MADO-AgNPs nanofiber.

days after treatment with MADO-AgNPs and MADO. The wounds without dressings were used as control, and the wound area was measured at certain times to determine the reduction in the wound area. In all groups, the size of the wound tends to decrease after treatment. After a 15-day treatment, the MADO-AgNPs showed a wound-healing ratio of 92%, which is higher than both that of MADO (65%) and the control group (51%). This excellent wound-healing effect could be attributed to the antibacterial performance of the releasable AgNPs, which provided a high level of antibacterial activity without inducing significant mammalian cell toxicity. The morphology of the nanofibers resembled extra cellular matrix (ECM) and supported a more intense cell growth while also providing the antibacterial effect, which altogether contributed to the activate wound care. It is worth mentioning that the rat wounds covered with MADO and MADO-AgNPs were distinguishable from those of control up to 5 days. The MADO and MADO-AgNPs animals were examined on day 15 and showed an improvement in the overall appearance of the wound, with a reduced inflammation indicated by a reduction in redness and minimal scarring. In contrast, the control animals either retained a portion of the scab or had shed it but exhibited a scarred, inflamed wound. By day 15, the wounds of the animals treated with MADO-AgNPs were not easily visible since no redness could be seen, and minimal scarring had occurred. At the same time, although the MADO group presented improved healing, the wounds still showed superficial signs of inflammation with a visible scar. This analysis further indicates that MADO-AgNPs provide better wound healing effects.

H&E was employed to evaluate the histological signs of the wound healing process. As shown in Figure 9, 15 days after the wound had been created, the control groups presented poor wound healing. However, the wound treated with MADO-AgNPs showed a complete glandular cavity, thickened epidermis, granular tissue formation, and big rete pegs as well as keratinocyte restoration. These improvements were observed with a less granular tissue formation and rete pegs on the wounds covered by the MADO nanofibers. These results indicate that the MADO-AgNPs dressings induced better wound healing than in the other groups.

CONCLUSION

Antibacterial electrospun nanofibers were developed to contain in situ-formed AgNPs without the addition of an external reducing agent, which is desirable to minimize the tissue toxicity. This method allows monodispersed AgNPs to be formed while allowing for the particle size and amount to be controlled. The AgNPs were characterized via TEM, XRD, and

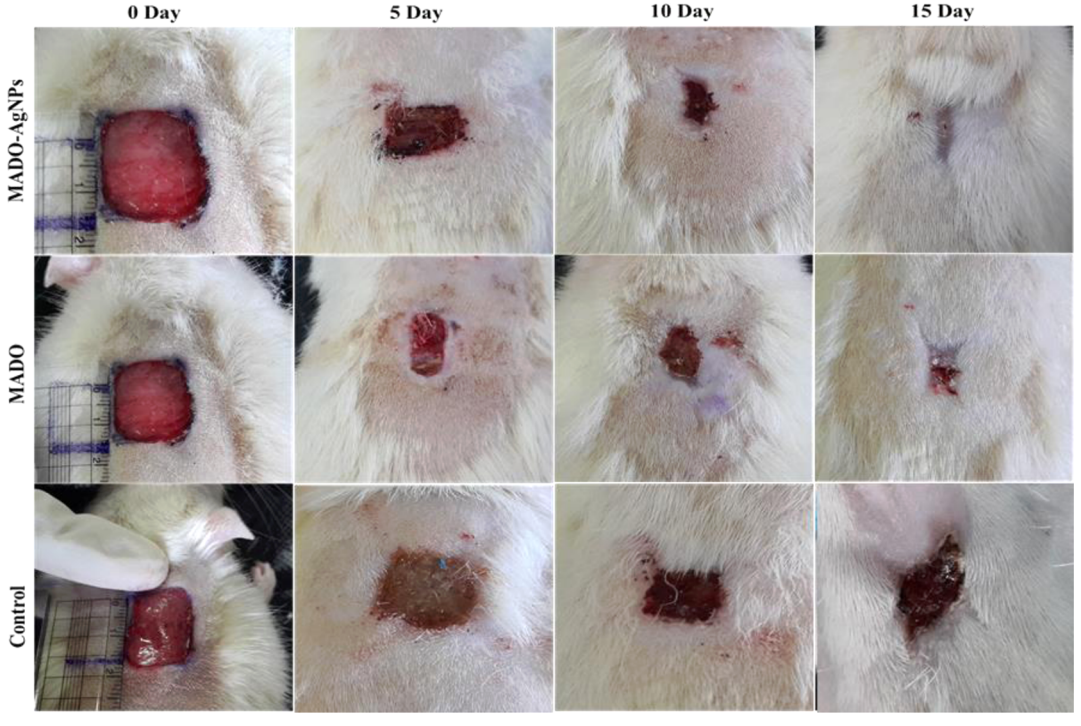

Figure 8. Wound appearance at 0, 5, 10, and 15 days after grafting with MADO-AgNPs, MADO nanofiber, and bare.

DOI: 10.1021/acsami.5b02542
ACS Appl. Mater. Interfaces 2015, 7, 12176−12183

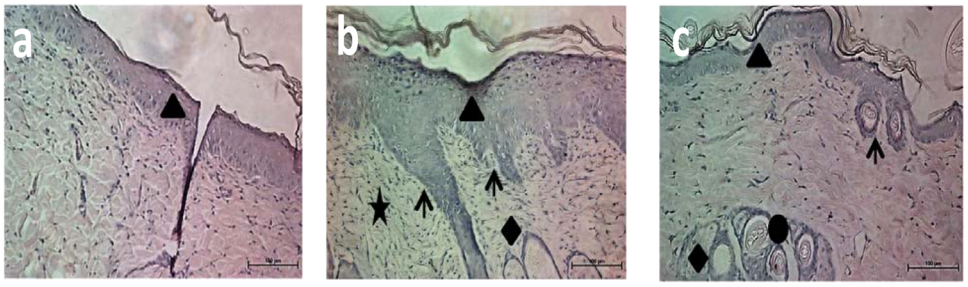

Figure 9. Sections of 15-day-old wounds stained with H&E. (a) Control: The epithelium control wounds are incomplete and remained flat over the wound bed. For (b) MADO-AgNPs and (c) MADO, the newly formed epithelium invaded into the granulation tissue to form rete pegs (the triangle, arrow, star, quadrangle, and circle indicate epidermis, rete pegs, granular tissue, glands, and blood vessels, respectively).

XPS, and monodispersed particles with diameters of less than 20 nm were obtained after incubation with 1 mM silver nitrate solution for 6 h. However, the pdopa-coated samples did not allow for the amount of particles to be controlled due to the existence of unavoidable pdopa macro/nanaoparticles during film formation.

The MADO-AgNPs composite nanofibers containing 1% NPs were observed to achieve desirable antibacterial activity against both Gram-negative and Gram-positive bacteria while not significantly affecting the viability of mammalian cells. We also observed a rapid release of the AgNPs within 24 h and a sustained release for 5 days thereafter. Such a sustained release of silver is a crucial prerequisite to provide effective antibacterial therapy at specific concentrations. The in vitro and in vivo studies further confirmed the bioavailability and antimicrobial activity of MADO-AgNPs as potent materials for wound-healing dressings.

■ ASSOCIATED CONTENT

Supporting Information

Availability of catechol hydroxyl groups in the MADO nanofibers observed by UV−vis spectroscopy. The Supporting Information is available free of charge on the ACS Publications website at DOI: 10.1021/acsami.5b02542.

■ AUTHOR INFORMATION

Corresponding Authors

*E-mail: chskim@jbnu.ac.kr. Phone: +82 63 270 4284. Fax: +82 63 270 2460.
*E-mail: biochan@jbnu.ac.kr.
*E-mail: ghavaminejad@jbnu.ac.kr.

Author Contributions

¶These authors contributed equally.

Notes

The authors declare no competing financial interest.

■ ACKNOWLEDGMENTS

This research was supported by grants from the Basic Science Research Program through the National Research Foundation of Korea (NRF), funded by the Ministry of Education, Science, and Technology (Project Nos. 2013-012911 and 2013R1A2A2A04015484). The authors would like to thank the staff of the CBNU central lab, Yeon-Soo Han and Pang, Su-Jin for help with NMR and ICP/MASS.

■ REFERENCES

(1) Pomahac, B.; Svensjo, T.; Yao, F.; Brown, H.; Eriksson, E. Tissue Engineering of Skin. *Crit. Rev. Oral Biol. Med.* **1998**, *9*, 333−344.
(2) Gurtner, G. C.; Werner, S.; Barrandon, Y.; Longaker, M. T. Wound Repair and Regeneration. *Nature* **2008**, *453*, 314−321.
(3) Barrientos, S.; Stojadinovic, O.; Golinko, M. S.; Brem, H.; Tomic-Canic, M. Growth Factors and Cytokines in Wound Healing. *Wound Repair Regen.* **2008**, *16*, 585−601.
(4) Wang, L. S.; Chow, P. Y.; Phan, T. T.; Lim, I. J.; Yang, Y. Y. Fabrication and Characterization of Nanostructured and Thermosensitive Polymer Membranes for Wound Healing and Cell Grafting. *Adv. Funct. Mater.* **2006**, *16*, 1171−1178.
(5) Rujitanaroj, P. O.; Pimpha, N.; Supaphol, P. Wound-Dressing Materials with Antibacterial Activity from Electrospun Gelatin Fiber Mats Containing Silver Nanoparticles. *Polymer* **2008**, *49*, 4723−4732.
(6) Fu, S. Z.; Meng, X. H.; Fan, J.; Yang, L. L.; Wen, Q. L.; Ye, S. J.; Lin, S.; Wang, B. Q.; Chen, L. L.; Wu, J. B.; Chen, Y.; Fan, J. M.; Li, Z. Acceleration of Dermal Wound Healing by Using Electrospun Curcumin-Loaded Poly(epsilon-caprolactone)-poly(ethylene glycol)-poly(epsilon-caprolactone) Fibrous Mats. *J. Biomed. Mater. Res. B* **2014**, *102*, 533−542.
(7) Khil, M. S.; Cha, D. I.; Kim, H. Y.; Kim, I. S.; Bhattarai, N. Electrospun Nanofibrous Polyurethane Membrane as Wound Dressing. *J. Biomed. Mater. Res. B* **2003**, *67B*, 675−679.
(8) Schwartz, V. B.; Thetiot, F.; Ritz, S.; Putz, S.; Choritz, L.; Lappas, A.; Forch, R.; Landfester, K.; Jonas, U. Antibacterial Surface Coatings from Zinc Oxide Nanoparticles Embedded in Poly(N-isopropylacrylamide) Hydrogel Surface Layers. *Adv. Funct. Mater.* **2012**, *22*, 2376−2386.
(9) Li, C. W.; Fu, R. Q.; Yu, C. P.; Li, Z. H.; Guan, H. Y.; Hu, D. Q.; Zhao, D. H.; Lu, L. C. Silver Nanoparticle/Chitosan Oligosaccharide/Poly(vinyl alcohol) Nanofibers as Wound Dressings: A Preclinical Study. *Int. J. Nanomed.* **2013**, *8*, 4131−4145.
(10) Charernsriwilaiwat, N.; Rojanarata, T.; Ngawhirunpat, T.; Opanasopit, P. Electrospun Chitosan/Polyvinyl Alcohol Nanofiber Mats for Wound Healing. *Int. Wound J.* **2014**, *11*, 215−222.
(11) Rieger, K. A.; Birch, N. P.; Schiffman, J. D. Designing Electrospun Nanofiber Mats To Promote Wound Healing—A review. *J. Mater. Chem. B* **2013**, *1*, 4531−4541.
(12) Unnithan, A. R.; Barakat, N. A. M.; Pichiah, P. B. T.; Gnanasekaran, G.; Nirmala, R.; Cha, Y. S.; Jung, C. H.; El-Newehy, M.; Kim, H. Y. Wound-Dressing Materials with Antibacterial Activity from Electrospun Polyurethane-Dextran Nanofiber Mats Containing Ciprofloxacin HCl. *Carbohydr. Polym.* **2012**, *90*, 1786−1793.
(13) Unnithan, A. R.; Gnanasekaran, G.; Sathishkumar, Y.; Lee, Y. S.; Kim, C. S. Electrospun Antibacterial Polyurethane-Cellulose Acetate-Zein Composite Mats for Wound Dressing. *Carbohydr. Polym.* **2014**, *102*, 884−892.
(14) Agarwal, A.; Guthrie, K. M.; Czuprynski, C. J.; Schurr, M. J.; McAnulty, J. F.; Murphy, C. J.; Abbott, N. L. Polymeric Multilayers That Contain Silver Nanoparticles Can Be Stamped onto Biological Tissues To Provide Antibacterial Activity. *Adv. Funct. Mater.* **2011**, *21*, 1863−1873.
(15) Atiyeh, B. S.; Costagliola, M.; Hayek, S. N.; Dibo, S. A. Effect of Silver on Burn Wound Infection Control and Healing: Review of the Literature. *Burns* **2007**, *33*, 139−148.

(16) Fullenkamp, D. E.; Rivera, J. G.; Gong, Y. K.; Lau, K. H. A.; He, L. H.; Varshney, R.; Messersmith, P. B. Mussel-Inspired Silver-Releasing Antibacterial Hydrogels. *Biomaterials* **2012**, *33*, 3783−3791.
(17) Reithofer, M. R.; Lakshmanan, A.; Ping, A. T. K.; Chin, J. M.; Hauser, C. A. E. In Situ Synthesis of Size-Controlled, Stable Silver Nanoparticles within Ultrashort Peptide Hydrogels and Their Antibacterial Properties. *Biomaterials* **2014**, *35*, 7535−7542.
(18) Cong, Y.; Xia, T.; Zou, M.; Li, Z. N.; Peng, B.; Guo, D. Z.; Deng, Z. W. Mussel-Inspired Polydopamine Coating as a Versatile Platform for Synthesizing Polystyrene/Ag Nanocomposite Particles with Enhanced Antibacterial Activities. *J. Mater. Chem. B* **2014**, *2*, 3450−3461.
(19) Lee, S. J.; Heo, D. N.; Moon, J. H.; Ko, W. K.; Lee, J. B.; Bae, M. S.; Park, S. W.; Kim, J. E.; Lee, D. H.; Kim, E. C.; Lee, C. H.; Kwon, I. K. Electrospun Chitosan Nanofibers with Controlled Levels of Silver Nanoparticles. Preparation, Characterization, and Antibacterial Activity. *Carbohydr. Polym.* **2014**, *111*, 530−537.
(20) Huang, C. B.; Soenen, S. J.; Rejman, J.; Trekker, J.; Liu, C. X.; Lagae, L.; Ceelen, W.; Wilhelm, C.; Demeester, J.; De Smedt, S. C. Magnetic Electrospun Fibers for Cancer Therapy. *Adv. Funct. Mater.* **2012**, *22*, 2479−2486.
(21) Yang, Y.; Guo, Z.; Zhang, H.; Huang, D. Q.; Gu, J. L.; Huang, Z. H.; Kang, F. Y.; Hatton, T. A.; Rutledge, G. C. Electrospun Magnetic Carbon Composite Fibers: Synthesis and Electromagnetic Wave Absorption Characteristics. *J. Appl. Polym. Sci.* **2013**, *127*, 4288−4295.
(22) Baker, C.; Pradhan, A.; Pakstis, L.; Pochan, D. J.; Shah, S. I. Synthesis and Antibacterial Properties of Silver Nanoparticles. *J. Nanosci. Nanotechnol.* **2005**, *5*, 244−249.
(23) Panacek, A.; Kvitek, L.; Prucek, R.; Kolar, M.; Vecerova, R.; Pizurova, N.; Sharma, V. K.; Nevecna, T.; Zboril, R. Silver Colloid Nanoparticles: Synthesis, Characterization, and Their Antibacterial Activity. *J. Phys. Chem. B* **2006**, *110*, 16248−16253.
(24) Ouyang, L.; Dotzauer, D. M.; Hogg, S. R.; Macanas, J.; Lahitte, J. F.; Bruening, M. L. Catalytic Hollow Fiber Membranes Prepared Using Layer-by-Layer Adsorption of Polyelectrolytes and Metal Nanoparticles. *Catal. Today* **2010**, *156*, 100−106.
(25) Macanas, J.; Ouyang, L.; Bruening, M. L.; Munoz, M.; Remigy, J. C.; Lahitte, J. F. Development of Polymeric Hollow Fiber Membranes Containing Catalytic Metal Nanoparticles. *Catal. Today* **2010**, *156*, 181−186.
(26) Son, H. Y.; Ryu, J. H.; Lee, H.; Nam, Y. S. Silver−Polydopamine Hybrid Coatings of Electrospun Poly(vinyl alcohol) Nanofibers. *Macromol. Mater. Eng.* **2013**, *298*, 547−554.
(27) Lee, H.; Dellatore, S. M.; Miller, W. M.; Messersmith, P. B. Mussel-Inspired Surface Chemistry for Multifunctional Coatings. *Science* **2007**, *318*, 426−430.
(28) Vatankhah-Varnoosfaderani, M.; GhavamiNejad, A.; Hashmi, S.; Stadler, F. J. Mussel-Inspired pH-Triggered Reversible Foamed Multi-Responsive Gel—The Surprising Effect of Water. *Chem. Commun.* **2013**, *49*, 4685−4687.
(29) Lee, Y.; Park, T. G. Facile Fabrication of Branched Gold Nanoparticles by Reductive Hydroxyphenol Derivatives. *Langmuir* **2011**, *27*, 2965−2971.
(30) Marcelo, G.; Lopez-Gonzalez, M.; Mendicuti, F.; Tarazona, M. P.; Valiente, M. Poly(N-isopropylacrylamide)/Gold Hybrid Hydrogels Prepared by Catechol Redox Chemistry. Characterization and Smart Tunable Catalytic Activity. *Macromolecules* **2014**, *47*, 6028−6036.
(31) Yang, H. W.; Lan, Y.; Zhu, W.; Li, W. N.; Xu, D.; Cui, J. C.; Shen, D. Z.; Li, G. T. Polydopamine-Coated Nanofibrous Mats as a Versatile Platform for Producing Porous Functional Membranes. *J. Mater. Chem.* **2012**, *22*, 16994−17001.
(32) Kim, H. W.; McCloskey, B. D.; Choi, T. H.; Lee, C.; Kim, M. J.; Freeman, B. D.; Park, H. B. Oxygen Concentration Control of Dopamine-Induced High Uniformity Surface Coating Chemistry. *ACS Appl. Mater. Interfaces* **2013**, *5*, 233−238.
(33) Wang, J. L.; Li, B. C.; Li, Z. J.; Ren, K. F.; Jin, L. J.; Zhang, S. M.; Chang, H.; Sun, Y. X.; Ji, J. Electropolymerization of Dopamine for Surface Modification of Complex-Shaped Cardiovascular Stents. *Biomaterials* **2014**, *35*, 7679−7689.
(34) Hong, S.; Kim, J.; Na, Y. S.; Park, J.; Kim, S.; Singha, K.; Im, G. I.; Han, D. K.; Kim, W. J.; Lee, H. Poly(norepinephrine): Ultrasmooth Material-Independent Surface Chemistry and Nanodepot for Nitric Oxide. *Angew. Chem., Int. Ed.* **2013**, *52*, 9187−9191.
(35) Mohammad, A. M.; Abdelrahman, A. I.; El-Deab, M. S.; Okajima, T.; Ohsaka, T. On the Aggregation Phenomena of Au Nanoparticles: Effect of Substrate Roughness on the Particle Size. *Colloid Surface A* **2008**, *318*, 78−83.
(36) Vatankhah-Varnoosfaderani, M.; Hashmi, S.; GhavamiNejad, A.; Stadler, F. J. Rapid Self-Healing and Triple Stimuli Responsiveness of a Supramolecular Polymer Gel Based on Boron−Catechol Interactions in a Novel Water-Soluble Mussel-Inspired Copolymer. *Polym. Chem.* **2014**, *5*, 512−523.
(37) GhavamiNejad, A.; Sasikala, A. R. K.; Unnithan, A. R..; Thomas, R. G.; Jeong, Y. Y.; Vatankhah-Varnoosfaderani, M.; Stadler, F. J.; Park, C. H.; Kim, C. S. Mussel-Inspired Electrospun Smart Magnetic Nanofibers for Hyperthermic Chemotherapy. *Adv. Funct. Mater.* **2015**, *35*, 2867−2875.
(38) Ma, Y. R.; Niu, H. Y.; Zhang, X. L.; Cai, Y. Q. One-Step Synthesis of Silver/Dopamine Nanoparticles and Visual Detection of Melamine in Raw Milk. *Analyst* **2011**, *136*, 4192−4196.
(39) Singho, N. D.; Lah, N. A. C.; Johan, M. R.; Ahmad, R. FTIR Studies on Silver−Poly(methylmethacrylate) Nanocomposites via in Situ Polymerization Technique. *Int. J. Electrochem. Sci.* **2012**, *7*, 5596−5603.
(40) Song, J.; Kang, H.; Lee, C.; Hwang, S. H.; Jang, J. Aqueous Synthesis of Silver Nanoparticle Embedded Cationic Polymer Nanofibers and Their Antibacterial Activity. *ACS Appl. Mater. Interfaces* **2012**, *4*, 460−465.
(41) Liang, M.; Su, R. X.; Huang, R. L.; Qi, W.; Yu, Y. J.; Wang, L. B.; He, Z. M. Facile in Situ Synthesis of Silver Nanoparticles on Procyanidin-Grafted Eggshell Membrane and Their Catalytic Properties. *ACS Appl. Mater. Interfaces* **2014**, *6*, 4638−4649.
(42) Kong, H.; Jang, J. Synthesis and Antimicrobial Properties of Novel Silver/Polyrhodanine Nanofibers. *Biomacromolecules* **2008**, *9*, 2677−2681.
(43) Black, K. C. L.; Sileika, T. S.; Yi, J.; Zhang, R.; Rivera, J. G.; Messersmith, P. B. Bacterial Killing by Light-Triggered Release of Silver from Biomimetic Metal Nanorods. *Small* **2014**, *10*, 169−178.
(44) Ku, S. H.; Park, C. B. Human Endothelial Cell Growth on Mussel-Inspired Nanofiber Scaffold for Vascular Tissue Engineering. *Biomaterials* **2010**, *31*, 9431−9437.
(45) Ku, S. H.; Ryu, J.; Hong, S. K.; Lee, H.; Park, C. B. General Functionalization Route for Cell Adhesion on Nonwetting Surfaces. *Biomaterials* **2010**, *31*, 2535−2541.
(46) Wang, H. R.; Cheng, M.; Hu, J. M.; Wang, C. H.; Xu, S. S.; Han, C. C. Preparation and Optimization of Silver Nanoparticles Embedded Electrospun Membrane for Implant Associated Infections Prevention. *ACS Appl. Mater. Interfaces* **2013**, *5*, 11014−11021.

DOI: 10.1021/acsami.5b02542
ACS Appl. Mater. Interfaces 2015, 7, 12176−12183